International Journal of Solids and Structures 51 (2014) 3431–3438

Contents lists available at ScienceDirect

International Journal of Solids and Structures

journal homepage: www.elsevier.com/locate/ijsolstr

Constitutive modelling of the amplitude and frequency dependency of filled elastomers utilizing a modified Boundary Surface Model

Rickard Österlöf [a,c,*], Henrik Wentzel [b], Leif Kari [a], Nico Diercks [d], Daniel Wollscheid [d]

[a] KTH Royal Institute of Technology, The Marcus Wallenberg Laboratory for Sound and Vibration Research (MWL), Centre for ECO² Vehicle Design, SE-100 44 Stockholm, Sweden
[b] KTH Royal Institute of Technology, Department of Solid Mechanics, SE-100 44 Stockholm, Sweden
[c] Scania, SE-151 87 Södertälje, Sweden
[d] University of the Bundeswehr München, Institute of Mechanics, 85579 Neubiberg, Germany

ARTICLE INFO

Article history:
Received 12 March 2014
Received in revised form 16 May 2014
Available online 14 June 2014

Keywords:
Filled elastomers
Amplitude dependency
Fletcher–Gent Effect
Carbon black
Natural rubber
Boundary Surface Model

ABSTRACT

A phenomenological uniaxial model is derived for implementation in the time domain, which captures the amplitude and frequency dependency of filled elastomers. Motivated by the experimental observation that the frequency dependency is stronger for smaller strain amplitudes than for large ones, a novel material model is presented. It utilizes a split of deformation between a generalized Maxwell chain in series with a bounding surface plasticity model with a vanishing elastic region. Many attempts to capture the behaviour of filled elastomers are found in the literature, which often utilize an additive split between an elastic and a history dependent element, in parallel. Even though some models capture the storage and loss modulus during sinusoidal excitations, they often fail to do so for more complex load histories. Simulations with the derived model are compared to measurements in simple shear on a compound of carbon black filled natural rubber used in driveline isolators in the heavy truck industry. The storage and loss modulus from simulations agree very well with measurements, using only 7 material parameters to capture 2 decades of strain (0.5–50% shear strain) and frequency (0.2–20 Hz). More importantly, with material parameters extracted from the measured storage and loss modulus, measurements of a dual sine excitation are well replicated. This enables realistic operating conditions to be simulated early in the development process, before an actual prototype is available for testing, since the loads in real life operating conditions frequently are a combination of many harmonics.

1. Introduction

Rising fuel prices, an increased environmental awareness and legal demands are incentives for the automotive industry to reduce fuel consumption, which efficiently lowers both costs and emissions. This reduction is achieved by for instance, lower revolutions at cruising speed, start-stop functionality, fuel cells, hybrid engines and lighter vehicles. At the same time, the demands on noise, vibration and harshness characteristics are ever increasing. Driveline isolators and rubber bushings have to be designed to fulfil these demands regardless of which driveline is used. In order to reduce cost and development time, computer aided simulations are used in the design process. However, the results of such simulations are, at most, only as good as the material models employed.

Almost all bushings, vibration isolators and shock absorbers in automotive vehicles are made out of elastomers. Elastomers' unique properties of high extensibility, damping and the introduction of a significant change in impedance make it ideal for the task of isolating the vibrations from the combustion engine and uneven roads (Sjöberg and Kari, 2002). However, in order to achieve sufficient stiffness, tear strength and an increased fatigue resistance, a reinforcing filler is often used (Heinrich et al., 2002).

For temperatures above the glass transition temperature unfilled elastomers have a stress–strain behaviour that for moderate, quasi-static, strains can be described by statistical and continuum mechanics (Boyce and Arruda, 2000; Treloar, 2005; Edwards and Vilgis, 1998). The addition of a reinforcing filler to the material introduces a strong strain amplitude dependency commonly referred to as the Fletcher–Gent effect, which is significant for strains larger than 0.01–0.1% (Fletcher and Gent, 1953; Payne and part, 1962; Kraus, 1984; Rendek and Lion, 2010; Wrana and Härtel, 2008). Therefore, the classical material models for unfilled elastomers are inadequate. Even more cumbersome, the response

* Corresponding author. Address: Scania CV AB, SE-151 87 Södertälje, Sweden. Tel.: +46 855353482.
E-mail address: rickard.osterlof@scania.com (R. Österlöf).

http://dx.doi.org/10.1016/j.ijsolstr.2014.06.003
0020-7683/

of a filled elastomer subjected to two simultaneous sinusoidal displacements does not equal the sum of the responses of the individual excitations (Wrana and Härtel, 2008; Sjöberg and Kari, 2003). Consequently, it is not an easy task to formulate an accurate material model in the frequency domain or calculate the response using Fourier methods since the superposition principle is not valid. Therefore, it is beneficial to formulate constitutive equations in the time domain. Furthermore, the vulcanization process and thereby the rubber compound are often undisclosed which means that the information needed for determining material parameters from the physical structure of the material would generally be unavailable. Hence, a phenomenological approach is advantageous when modelling filled elastomers with material parameters that can be deduced from small test samples and simple experiments.

A method frequently used to model filled elastomers is to additively decompose it into an elastic part and a history-dependent part, in parallel. The simplest model that combines relaxation with a stiffness at quasi-static loading conditions is the well known standard linear solid (SLS). However, measurements have shown that vulcanized filled elastomers contain a spectrum of relaxation times (Adolfsson et al., 2005; Lion, 1998) where the SLS for obvious reasons is limited to a single relaxation time. For a finite range of frequencies, this can be modelled by adding more Maxwell elements in parallel to the SLS, resulting in a generalized Maxwell chain (GMC). Another way of capturing a spectrum of relaxation times is with fractional derivatives (Adolfsson et al., 2005). The major drawback of fractional derivatives is that the results from all previous time steps are needed for the calculation of the next, which makes it computationally expensive. Even though this to some extent has been solved by implementing a sparse time history (Adolfsson et al., 2004; Adolfsson, 2004), neither fractional derivatives nor the conventional GMC have the ability to capture the observed amplitude dependency of filled elastomers, without modifications.

By utilizing non-linear viscoelastic models with process dependent relaxation times an amplitude dependency can be introduced (Rendek and Lion, 2010; Höfer and Lion, 2009; Liu and Fatt, 2011). However, choosing evolution laws for the internal variables is often a complicated matter with many material parameters to define, which often leads to a trade-off if the storage or the loss modulus should be represented accurately.

Another technique often used to model the Fletcher–Gent effect is with plastic elements. For uniaxial loading conditions, many models exist that capture the smooth plastic behaviour of filled elastomers, one being the standard triboelastic solid (Coveney et al., 1995; Coveney and Johnson, 1999). The strength of this and similar models (Berg, 1995; Dahl et al., 1960; Netzker et al., 2010) is that the amplitude dependency of the complex modulus can be well reproduced, but their main drawback is the absence of frequency dependency. This problem is addressed either by adding a strain rate dependency in the plastic element (Coveney and Johnson, 2000; Hu and Wereley, 2012) or by adding for instance a fractional derivative (Sjöberg and Kari, 2002; García Tárrago et al., 2007) or a GMC (Yarmohamadi and Berbyuk, 2010; Gracia et al., 2010) in parallel to the elastoplastic model.

For the finite element method, there exist phenomenological constitutive equations implemented for three-dimensional analysis that capture the amplitude dependency and hysteresis in filled elastomers for large deformations, such as the MORPH-model (Besdo and Ihlemann, 2003) or an endochronic plasticity formulation (Netzker et al., 2010). Unfortunately these material models have no strain rate dependency, but this can be improved by using an overlay method (Gracia et al., 2010) and a viscoelastic model suitable for large deformations (Govindjee and Reese, 1997; Bergström and Boyce, 1998).

However, measurements in literature clearly show that when the frequency is increased, the increase in stiffness in absolute values is larger for smaller strain amplitudes (Sjöberg and Kari, 2002; Rendek and Lion, 2010; Lion and Kardelky, 2004; Chazeu et al., 2000; Luo et al., 2010). This is a strong indication that an additive split between plastic and viscous elements is not an accurate approach in a material model with the ambition to capture the response in filled elastomers. From a physical point of view, it is acknowledged that the Fletcher–Gent effect is caused not solely from the breakdown and reforming of filler-filler structures, but that there is a substantial contribution from filler-polymer interactions (Ahmadi and Muhr, 2011; Donnet and Custodero, 2013; Fröhlich et al., 2005; Litvinov et al., 2011). This is interpreted as polymer chains in series with a mechanism which causes energy dissipation, which again suggests that a polymer network in series with a plastic contribution is suitable for modelling filled elastomers.

In this paper, a constitutive model for filled elastomers is presented, with the novelty being an addition of a frequency dependency to the bounding surface model with a vanishing elastic region (Dafalias and Popov, 1977). The derived model will be compared to measurements on a compound of carbon black filled natural rubber, used as isolators in the heavy truck industry. Finally, the model proposed is intended for the evaluation of the dynamical behaviour of rubber compounds with reinforcing fillers. If the stresses and strains are reproduced well, the durability of a component and the surrounding structure has the potential to be optimized. For many load bearing components made out of rubber, the strains are typically moderate to large (50% shear strain is not uncommon) and in the lower frequency domain (typically below 20 Hz). This calls for a material model that can handle large perturbations from an equilibrium condition. However, it needs only to be accurate in a relatively small frequency bandwidth (0.2–20 Hz). Also, in the intended application, the strains are not expected to be large enough for the finite extensibility of the polymer chains to influence the dynamical stiffness of the components. Such high strain amplitudes could result in an unacceptably low durability (Sheridan et al., 2001).

The presented model enables the properties of components subjected to uniaxial loading conditions to be studied via simulations before an actual prototype is available for testing, given that small test specimens to determine material parameters are often accessible early in the design process.

2. Measurements

The measurements are conducted in a GABO EPLEXOR® 500 N, fitted with a force transducer with a measurement range of 150 N. The experimental setup and the dimensions of the rubber specimen are shown in Fig. 1. The rubber was injection moulded between steel parts, the two outward pieces were attached to a baseplate and a displacement is applied via the middle piece,

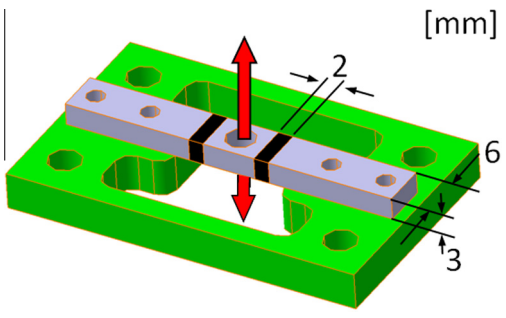

Fig. 1. Test specimen. Rubber compound vulcanized between three steel pieces. Displacement applied on middle piece.

effectively shearing the rubber. Measurements are made of the applied displacement and the resulting force. There is a geometrical influence on the measured shear modulus of the material since the width-to-height ratio of the rubber is only 1.5, whereas it should be at least 5 when material parameters are to be obtained (Rubber, 2011). However, the objective of this paper is to derive a material model for filled elastomers and not to determine the parameters for a specific compound. To this end the measurement data is sufficiently accurate, with less than 15% difference in the magnitude of the shear modulus. This was determined by modelling the experimental setup in Abaqus, and using a linear, incompressible, material model in a non-linear finite strain calculation. The shear stress required for a certain amount of shear strain was compared to the true shear modulus of the material. Table 1 shows the composition of the compound, labelled NR3233 by the manufacturer TrelleborgVibracoustic.

The properties of the rubber compound are investigated prior to the formulation of the constitutive equations. Experiments are conducted in simple shear with a sinusoidal excitation at room temperature: 23°C. Before the start of measurements, the test specimen is subjected to five cycles with the maximum shear strain (50% shear strain), in order to reach a steady state so that the initial stress softening known as the Mullins effect (Mullins, 1969) is not included in the measurements. Thereafter, frequency sweeps in the range of 0.5–20 Hz are conducted with a constant strain amplitude. After each sweep, the amplitude is increased, and a new frequency sweep commences. The frequency sweeps with the initiating low frequency (0.1 Hz), large strain amplitudes, is shown in Fig. 2. The measured strain amplitudes are 0.2, 0.5, 1, 5, 10, 20 and 50% shear strain.

The stress response from a 50% shear strain, low frequency (0.1 Hz) excitation is shown in Fig. 3. As can be seen, there is no apparent increase in stiffness for large shear strains. Therefore, the assumption to not include the finite extensibility of the polymer chains in the model is deemed to be valid. Since the response is not a perfect sinusoidal, the hysteresis in Fig. 3 is not elliptical. Therefore, the classical definition of storage and loss modulus is inapplicable. In this work, the storage and loss modulus, G' and G'', are defined as

$$G' = \frac{\tau_{\text{amp}}}{\gamma_{\text{amp}}} \tag{1}$$

and

$$G'' = G' \tan \delta_{\text{eqv}}, \tag{2}$$

$\tan \delta_{\text{eqv}}$ is defined as

$$\tan \delta_{\text{eqv}} = W/(\pi \tau_{\text{amp}} \gamma_{\text{amp}}), \tag{3}$$

where δ_{eqv} is the equivalent loss angle and $W = \oint \tau \mathrm{d}\gamma$ is the dissipated energy during one cycle, where τ and γ is the measured stress and strain, respectively. The classical definition assumes that when the applied strain is harmonic, $\gamma(t) = \gamma_{\text{amp}} \cos \omega t$, the stress is also harmonic, with a phase shift, $\tau(t) = \tau_{\text{amp}} \cos(\omega t + \delta)$. The dissipated energy during one cycle is then given by

$$W = \oint \tau \mathrm{d}\gamma = \int^T \tau \dot{\gamma} \mathrm{d}t = -\tau_{\text{amp}} \gamma_{\text{amp}} \omega \int^T \sin \omega t \cos(\omega t + \delta) \mathrm{d}t$$
$$= \tau_{\text{amp}} \gamma_{\text{amp}} \pi \sin \delta \tag{4}$$

Table 1
Compounds in the rubber compound in parts per hundred rubber, by weight, and Shore A hardness.

NR [phr]	Filler [phr]	Plasticizer [phr]	Additives [phr]	Shore A
100	54	13	19	50

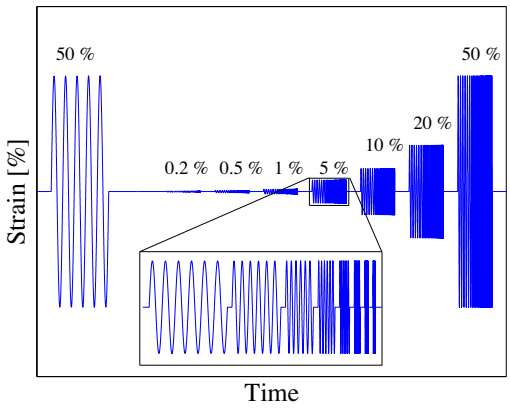

Fig. 2. Initial large strain, low frequency excitations, followed by frequency sweeps at increasing strain amplitudes.

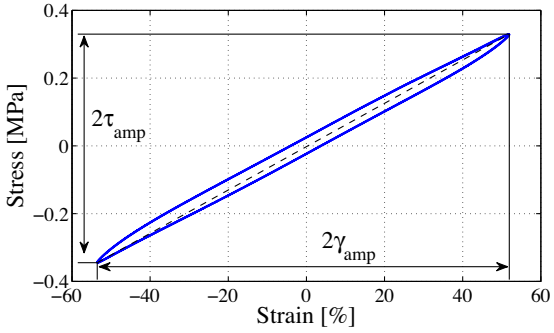

Fig. 3. Hysteresis for moderate amplitude, low frequency (0.1 Hz). Here, the storage modulus is defined as the secant modulus.

If the stress and strain are given in the complex plane as $\gamma^* = \gamma_{\text{amp}} e^{i\omega t}$ and $\tau^* = \tau_{\text{amp}} e^{i\omega t + \delta}$, the complex shear modulus is given as $G^* = \tau^*/\gamma^* = \tau_{\text{amp}}/\gamma_{\text{amp}} e^{i\delta}$. The complex modulus can then be separated into real and imaginary parts as $G^* = G' + iG'' = \tau_{\text{amp}}/\gamma_{\text{amp}} \cos \delta + i \tau_{\text{amp}}/\gamma_{\text{amp}} \sin \delta$, from where it follows that $G''/G' = \tan \delta$. If the measured response is purely sinusoidal, with a phase shift, and the loss angle is small, $\cos \delta \approx 1$, Eqs. (1)–(3) are good approximations to the classical definition of storage and loss modulus.

The storage and loss modulus in the measurements are calculated according to Eqs. (1) and (2) and shown in Fig. 4–7. The Fletcher–Gent effect is clearly visible. It can also be noted that the frequency dependency of the storage modulus in absolute values is larger for smaller strain amplitudes, which is the expected result. The same dependencies can be found in other measurements of filled elastomers (Sjöberg and Kari, 2002; Rendek and Lion, 2010; Lion and Kardelky, 2004; Chazeu et al., 2000; Luo et al., 2010). It is observed that the exact values of the loss modulus is uncertain for the smallest strain amplitudes due to a reduced signal-to-noise ratio. However, the results still show a general trend of the loss modulus, and they are therefore included in Figs. 5 and 7.

3. Constitutive modelling

The behaviour of filled elastomers is proposed to be modelled using a Boundary Surface Model with a vanishing elastic region (BSM) (Dafalias and Popov, 1977) with a modification that results from observation of measurements in the literature. Firstly, measurements with small strain amplitudes indicate the presence of

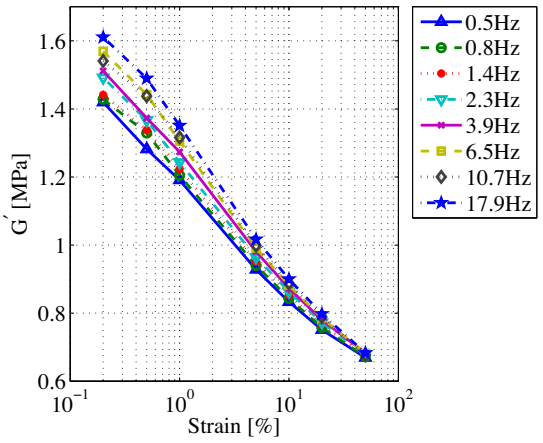

Fig. 4. Storage modulus as a function of strain.

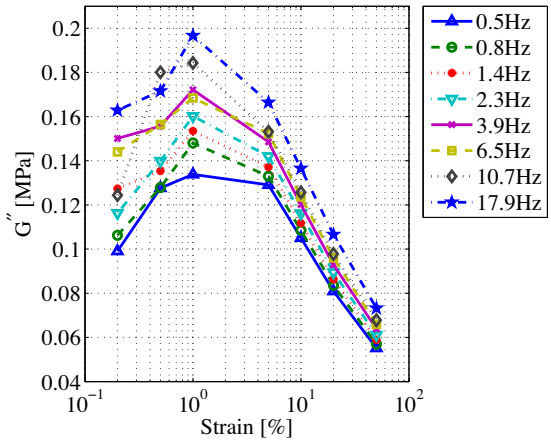

Fig. 5. Loss modulus as a function of strain.

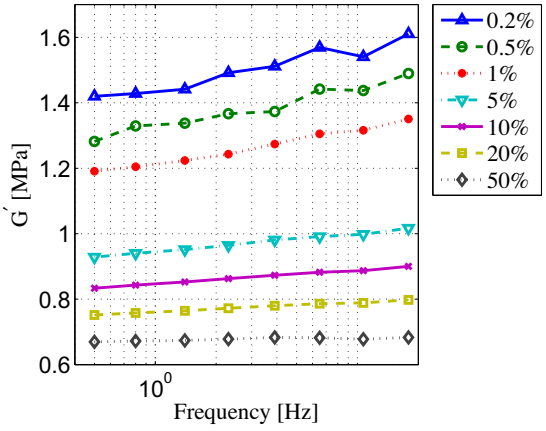

Fig. 6. Storage modulus as a function of frequency.

a plateau for which the stiffness remains unaffected when the strain amplitude of the excitation is further reduced (Payne and part, 1962; Rendek and Lion, 2010). For the BSM, the stiffness tends toward infinity in the limit when the strain amplitude tends toward zero as will be shown in Section 3.1. Therefore, it seems reasonable to place a finite stiffness in series with the BSM. A simple rheological equivalence is two springs in series where one has a non-linear stiffness which decreases with increasing amplitude of displacement and the other is of constant stiffness. Secondly, an

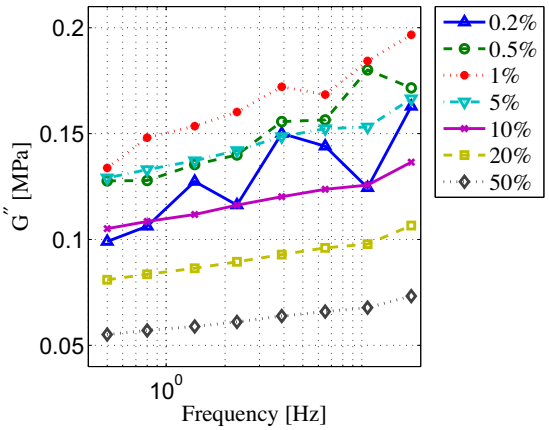

Fig. 7. Loss modulus as a function of frequency.

increase of frequency yields a higher increase in stiffness, in absolute values, for small strains than for large strains, which is apparent from the results shown in Fig. 4. These two observations suggest that a BSM in series with a GMC could be appropriate for modelling filled elastomers. A one-dimensional rheological model is shown in Fig. 8. The measured, total shear strain, γ, is the sum of the strain over the BSM, w, and the GMC, q, as $\gamma = q + w$.

The constitutive equations for the total stress in a GMC are well known,

$$\tau_{\text{tot}}(t) = q(t)G_\infty + \sum_{i=1}^{N} c_i \frac{\mathrm{d}q}{\mathrm{d}t} - \frac{c_i}{G_i}\frac{\mathrm{d}\tau_i}{\mathrm{d}t}, \tag{5}$$

where τ_i refers to the stress in the i-th Maxwell chain. However, the internal variable $q(t)$ is unknown. By noting that the stress is equal in the GMC and the plastic element, and by stating the evolution laws for the plastic behaviour, the stress resulting from an applied external strain can be derived.

3.1. Plastic behaviour

It is proposed to model the plastic behaviour with a constitutive law incorporating two yield surfaces: an interior surface and a bounding surface. The surfaces manifest purely kinematic hardening and the interior yield surface has a vanishing elastic region. Such a model was developed by Dafalias and Popov (1977) to model cyclic plasticity in metals. Here it is used to model the hysteresis exhibited by filled elastomers. For uniaxial loading several models exist that exhibit a smooth frictional behaviour, with no elastic region, suitable for cyclic loading conditions, e.g. the Berg and Dahl friction models (Berg, 1995; Dahl et al., 1960). The main advantage for using the proposed model is its ability to take irregular (non-sinusoidal) cyclic plastic loading in three dimensions into account.

The load process is defined by the incremental stress $\dot{\sigma}ij$, and the considered processes are isothermal. The yield surface f and boundary surface F are defined as

$$f(\sigma_{ij} - \alpha_{ij}) = 0 \tag{6}$$

and

$$F(\sigma_{ij} - \beta_{ij}) = 0, \tag{7}$$

where $\alpha_i j$ and $\beta_i j$ are back-stresses, i.e. they represent the centre of the yield surface and boundary surface, respectively. The surface f is located inside F, and the former is of vanishing size. The two surfaces translate simultaneously in stress space and may touch, but not intersect. In one dimension this can be visualized as in Fig. 9,

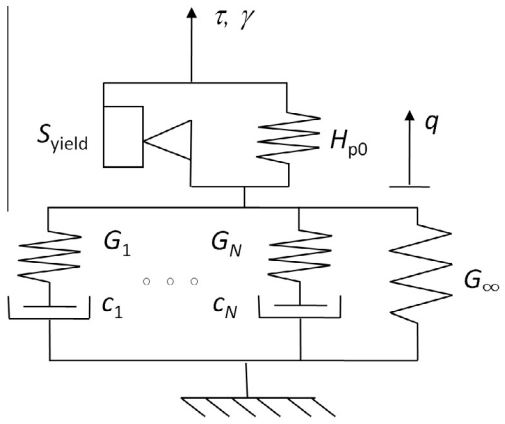

Fig. 8. Rheological model of carbon black filled natural rubber.

where there are two bounds XX' and YY' which limit the magnitude of stress. The boundaries are here represented with straight lines, but they could also be curved. For the evolution of the back stresses in three dimensions, the reader is referred to Dafalias and Popov (1977). For uniaxial loading, the evolution laws are simply (Ottosen and Ristinmaa, 2005, p. 342)

$$\dot{\tau} = H\dot{w} = \dot{\alpha} \tag{8}$$

and

$$\dot{\beta} = H_{p0}\dot{w} \tag{9}$$

with H being the plastic modulus, where H_{p0} is the value of the plastic modulus when the yield surface and boundary surface intersect. The expression for the plastic modulus may have many different forms. In this paper, one similar to Dafalias and Popov (1977) is used, namely,

$$H(\delta, \delta_{in}) = H_{p0}\left(1 + \frac{\delta}{\delta_{in} - \delta}\right), \tag{10}$$

where δ is the current distance to the boundary surface and δ_{in} is the distance to the boundary surface at the last turning point. Compared to the form of the plastic modulus in the original model, this is a simplified expression omitting a parameter that controls the shape of the hardening behaviour.

In displacement controlled simulations, the stress is calculated by combining the evolution laws for the GMC and the BSM. In the following, the value of a variable at time step t is denoted $(\cdot)_t$ and $(\cdot)_{t+1} = (\cdot)_t + \Delta(\cdot)_{t+1}$. With $w = \gamma - q$, the internal variable q is updated using an Euler forward method,

$$\Delta q_{t+1} = \frac{\Delta\gamma_{t+1} \cdot H_t + \sum_{i=1}^{n} \tau_{i|t} \frac{G_i}{c_i} dt}{G_\infty + H_t + \sum_{i=1}^{n} G_i}. \tag{11}$$

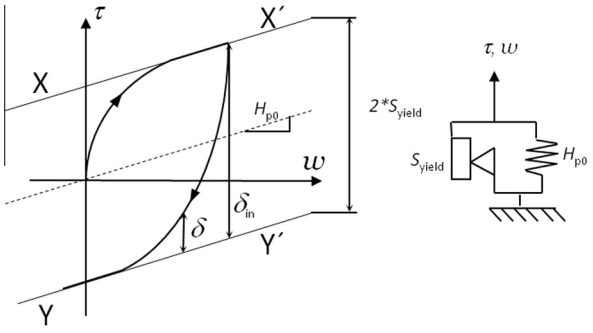

Fig. 9. The one-dimensional representation of a Boundary Surface Model with a vanishing elastic region.

A trial function for the incremental change of stress, $\Delta\tau^*$, in the plastic part of the model is computed for each time step as

$$\Delta\tau^*_{t+1} = (\Delta\gamma_{t+1} - \Delta q_{t+1}) \cdot H_t. \tag{12}$$

The loading direction l is $l_{t+1} = \Delta\tau^*_{t+1}/|\Delta\tau^*_{t+1}|$. If $l_{t+1} \cdot l_t < 0$, the load direction has changed, and the internal variable δ_{in} is updated as

$$\delta_{in} = S_{yield} \cdot l_{t+1} - (\tau_t - \beta_t). \tag{13}$$

Since the plastic modulus dramatically changes at load reversal, the trial function for the incremental change of stress is updated. The plastic modulus, Eq. (10), is unbounded at load reversal. With an implicit integration scheme this is not a problem because the algorithmic tangent modulus is bounded. With the current explicit scheme, this issue is managed by imposing a bound on the algorithmic tangent modulus, $H_t \leqslant H_{max}$, where $H_{max} = 100 \cdot G_\infty$, and G_∞ is the equilibrium stiffness of the GMC. As long as H_{max} is sufficiently larger than the stiffness in the GMC, applying an upper limit to H has an insignificant influence on the results. At load reversal, the internal variable and the trial function for the incremental stress are recalculated according to Eqs. (11) and (12), with $H_t = H_{max}$.

At the end of each time step, the distance to the boundary surface and the plastic modulus are updated as

$$\delta_{t+1} = S_{yield} l_{t+1} - (\tau_t - \beta_t + \Delta\tau^*_{t+1}), \tag{14}$$

$$H_{t+1} = H_{p0}\left(1 + \frac{\delta_{t+1}}{\delta_{in} - \delta_{t+1}}\right) \tag{15}$$

and

$$H_{t+1} = \min(H_{t+1}, H_{max}). \tag{16}$$

The actual stress and back stress are updated as

$$\Delta\tau_{t+1} = H_{t+1}(\Delta\gamma_{t+1} - \Delta q_{t+1}), \tag{17}$$

$$\Delta\beta_{t+1} = H_{p0}(\Delta\gamma_{t+1} - \Delta q_{t+1}), \tag{18}$$

$$\tau_{t+1} = \tau_t + \Delta\tau_{t+1} \tag{19}$$

and

$$\beta_{t+1} = \beta_t + \Delta\beta_{t+1}. \tag{20}$$

4. Obtaining material parameters

The proposed material model has $3 + 2N$ parameters $(S_{yield}, H_{p0}, G_\infty, G_1, \ldots, G_N, c_1, \ldots, c_N)$. Here, a method is presented to extract the material parameters based on test data. The method assumes that isothermal tests have been performed at the temperature of interest in the frequency and amplitude range of interest $[f_1, f_2]$ and $[a_1, a_2]$, respectively. Furthermore, it is assumed that no further increase in stiffness is observed if a_1 is lowered further. If the measured amplitude range is not sufficiently large, the material parameters acquired with the following scheme could be inaccurate. Nevertheless, the parameters will be in the right order of magnitude and are candidate starting points for further optimization, either numerically or manually.

Amplitudes below the range of interest are treated as infinitesimal, and at the lowest frequency, f_1, the stiffness is assumed to be completely determined by the parameter G_∞. For these measurements, it is therefore easily defined from Fig. 4 ($G_\infty = 1.4$ MPa). The parameters of the plastic element are obtained at low frequency, and the viscous effects are neglected, as discussed above. The dissipation is measured from $G''(f_1, a_2)$, and the parameter S_{yield} is chosen to fit the cyclic energy dissipation at large

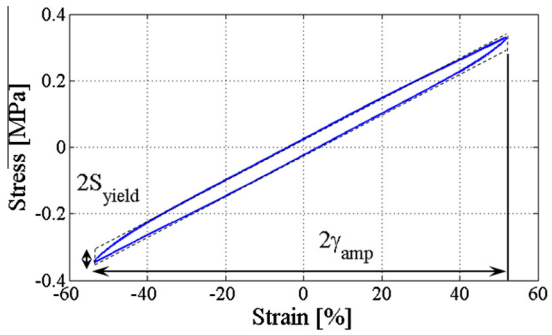

Fig. 10. The material parameter S_{yield} is found from the simplification that the dissipated energy can be calculated as the area of a parallelogram.

amplitudes and low frequencies, $2S_{yield} \cdot 2\gamma_{amp} = W(f_1, a_2)$. With the simplification that the dissipated energy can be computed as the area of the parallelogram in Fig. 10 and using Eqs. (1)–(3),

$$S_{yield} = \frac{\pi G''(f_1, a_2)\gamma_{amp}}{4}. \tag{21}$$

The model's large strain tangent stiffness, observed at large amplitudes and low frequencies $G'(f = f_1, a \to \infty)$ equals $H_{p0} \cdot G_\infty/(H_{p0} + G_\infty)$. This is the asymptotic value of G', which may or may not have converged at the amplitude a_2. It is proposed to choose H_{p0} according to

$$H_{p0} = \frac{(G'(f_1, a_2) - S_{yield}/\gamma_{amp})G_\infty}{G_\infty - G'(f_1, a_2) + S_{yield}/\gamma_{amp}}. \tag{22}$$

The stiffness in the Maxwell chains is for simplicity set to the same value, $G_i = G$, where $i = 1, 2, \ldots, N$. The value of G depends on the number of Maxwell chains and the characteristic frequencies $f_{c,i}$ for each chain i. A Maxwell chain has zero stiffness at quasi-static loading and equals the spring stiffness at frequencies well over the characteristic frequency f_c. As can be observed in Fig. 7, the measured loss modulus increases almost linearly as a function of frequency, on a logarithmic scale, for all amplitudes, even though the increase is very small for the large amplitudes. The loss modulus of a Maxwell chain has a maximum at f_c. This means that for one Maxwell chain, f_c needs to be set in the middle to upper end of the frequency range $[f_1, f_2]$. For two or more Maxwell chains, the loss modulus should not decrease in the frequency range of interest. The spring stiffness G is chosen such that the increase of stiffness for the Maxwell chains equals the difference between $G'(a_1, f_1)$ and $G'(a_1, f_2)$.

5. Results

As a first model, only one Maxwell element is used, with the characteristic frequency 4 Hz ($f_c = G/2\pi c$), which is in the middle of the frequency range, on a logarithmic scale. The smallest amplitude in the measurement is 0.2%, and the strain amplitude for which carbon black filled natural rubber experiences a plateau is found in the literature to be somewhere between 0.01–0.1% (Fletcher and Gent, 1953; Payne and part, 1962; Kraus, 1984; Rendek and Lion, 2010; Wrana and Härtel, 2008). As seen in Fig. 4, there is no apparent plateau in the storage modulus at the lowest strain amplitudes. Therefore, the G_∞ obtained trough the calibration scheme is underestimated. The parameters obtained were $S_{yield} = 0.022$ MPa, $H_{p0} = 1.13$ MPa, $G_\infty = 1.4$ MPa, $G = 0.2$ MPa, $f_c = 4$ Hz, and the results from this material model are shown in the middle graphs of Figs. 12 and 13. An optimization of the material parameters would surely give a better fit to the measurements. However, from the middle graph in Fig. 13, it is apparent that one Maxwell element is not enough to get the correct behaviour for the loss modulus. In order to get a good fit for the loss modulus over the frequency range of interest, three Maxwell elements are used. The calibration scheme in the previous section is still used since good starting points are needed for this highly non-linear optimization problem. Objective functions with different quotas between the measured and calculated storage and loss modulus are calculated as

$$\text{obj}_1 = \sum_{i=1}^{7}\sum_{j=1}^{8}\left(\ln\left(\frac{G'_{meas}(a_i, f_j)}{G'_{sim}(a_i, f_j)}\right)\right)^2, \tag{23}$$

$$\text{obj}_2 = \sum_{i=1}^{7}\sum_{j=1}^{8}\left(\ln\left(\frac{G''_{meas}(a_i, f_j)}{G''_{sim}(a_i, f_j)}\right)\right)^2, \tag{24}$$

$$\text{obj}_3 = \max\left(\ln\left(\frac{G'_{meas}(a_i, f_j)}{G'_{sim}(a_i, f_j)}\right)\right)^2 + \min\left(\ln\left(\frac{G'_{meas}(a_i, f_j)}{G'_{sim}(a_i, f_j)}\right)\right)^2 \tag{25}$$

and

$$\text{obj}_4 = \max\left(\ln\left(\frac{G''_{meas}(a_i, f_j)}{G''_{sim}(a_i, f_j)}\right)\right)^2 + \min\left(\ln\left(\frac{G''_{meas}(a_i, f_j)}{G''_{sim}(a_i, f_j)}\right)\right)^2 \tag{26}$$

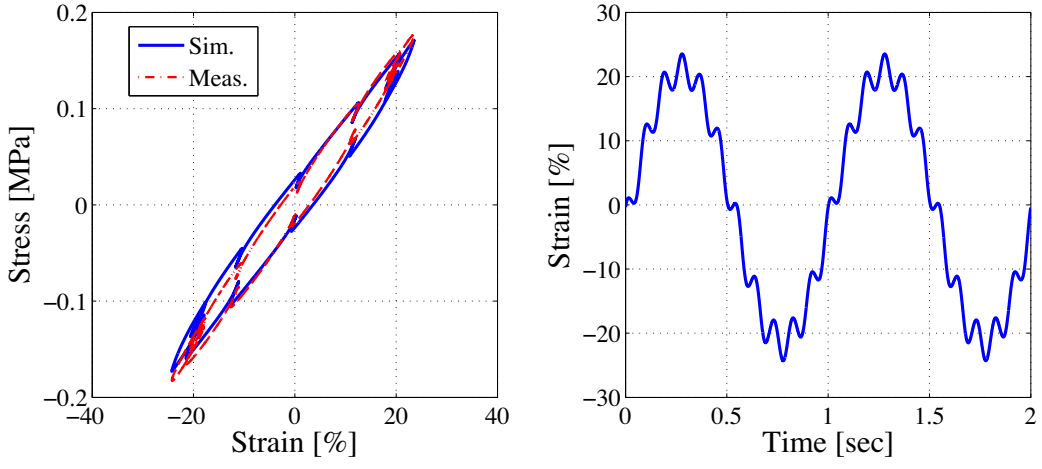

Fig. 11. Simulation and measurement of dual sine excitation.

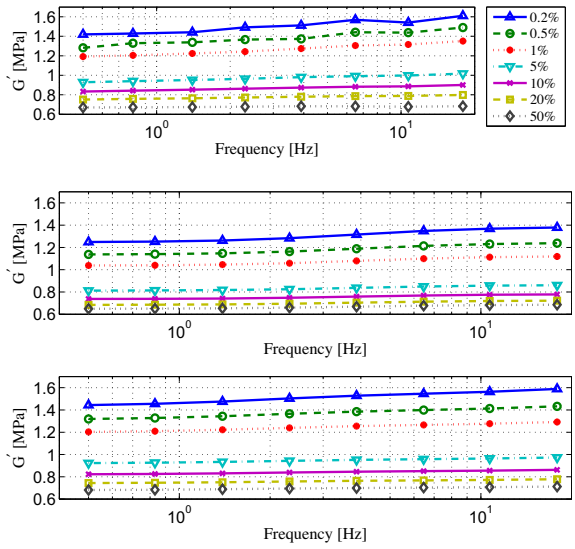

Fig. 12. Storage modulus from simulations and measurements. Top: measurements. Middle: one Maxwell element. Bottom: three Maxwell elements.

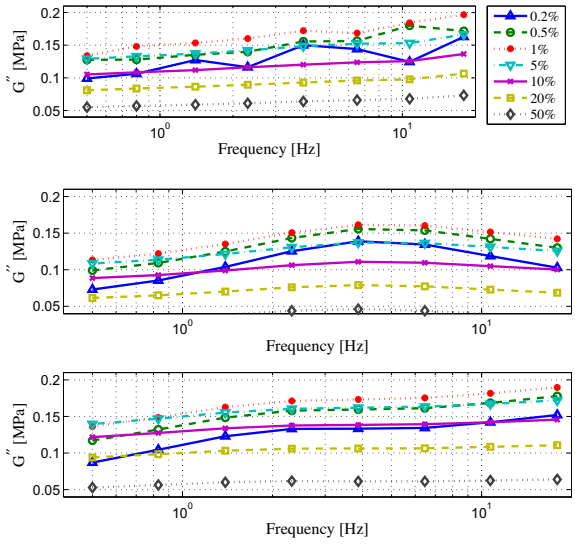

Fig. 13. Loss modulus from simulations and measurements. Top: measurements. Middle: one Maxwell element. Bottom: three Maxwell elements.

and are minimized using the commercial optimization software HEEDS® MDO (Red Cedar Technology, Inc., East Lansing, MI, USA).

The final material parameters obtained are $S_{yield} = 0.037$ MPa, $H_{p0} = 1.06$ MPa, $G_\infty = 1.59$ MPa, $G = 0.146$ MPa, $f_{c1} = 171$ Hz, $f_{c2} = 21$ Hz *and* $f_{c3} = 1.9$ Hz. The calculated storage and loss modulus are shown in the bottom graphs of Figs. 12 and 13. The amplitude dependency on the loss modulus is captured in the presented material model, with a maximum around 1% strain amplitude.

5.1. Comparing with bimodal excitation

Using the material parameters above, the model with three Maxwell chains is subjected to a dual sine excitation, and the results are compared to the response from measurements. The results are displayed in Fig. 11 and as seen the simulated response resembles the measurement well.

6. Discussion

By utilizing a split of deformation between elastoplastic in series with viscoelastic elements, the measured loss and storage modulus are reproduced very well by simulations. Also, and of greater importance, the measured and simulated response to a bimodal excitation are in good agreement, even though the bimodal measurements were not used when obtaining the material parameters. In order to model the finite extensibility of polymer chains, one possibility could be to replace the linear stiffness H_{p0} and G_∞ with non-linear elements. However, since this phenomenon is negligible for the studied range of strain amplitudes, this has not been investigated further.

In this work the model has been implemented uni-axially and compared to uniaxial test data. The simplicity of the proposed model together with the accurate results it yields makes it ideal for modelling filled rubber-bushings subjected to uniaxial loading. The non-linear stiffness and damping of these bushings strongly influence the response in the complete vehicle, and the loading is rarely sinusoidal. For components subjected to shear, the model can facilitate design engineers in choosing between concepts and geometries, early in the design phase. For more complex geometries and loading conditions, the model should be expanded into three dimensions. Even though the individual rheological elements, the GMC and the BSM, have three-dimensional equivalents, the task is not trivial, and will be the focus of future research. Nevertheless, many bushings and isolators are primarily sheared in one plane, and the derived uniaxial model can be expanded to two dimensions by implementing two uniaxial models on that plane, perpendicular to each other, since the influence of a pre-load in shear is relatively weak (Heinrich and Klüppel, 2002).

By limiting the model's applicability to a finite range of frequencies and amplitudes, the number of material parameters can be kept to a minimum, without reducing the models usability. In this paper, the limiting range of frequencies and amplitudes was 0.5–20 Hz and 0.2–50% shear strain, which is deemed more than sufficient when investigating the high amplitude dynamic loads on bushings and vibration isolators in, for instance, heavy truck applications.

Acknowledgements

The work presented in this paper has been carried out within the Centre for ECO^2 Vehicle Design at KTH, Stockholm. The financial support from the centre and from Scania CV AB is gratefully acknowledged.

References

Adolfsson, K., 2004. Nonlinear fractional order viscoelasticity at large strains. Nonlinear Dyn. 38, 233–246.
Adolfsson, K., Enelund, M., Larsson, S., 2004. Adaptive discretization of fractional order viscoelasticity using sparse time history. Comput. Methods Appl. Mech. Eng. 193, 4567–4590.
Adolfsson, K., Enelund, M., Olsson, P., 2005. On the fractional order model of viscoelasticity. Mech. Time-Depend. Mater. 9, 15–34.
Ahmadi, H., Muhr, A., 2011. Dynamic properties of filled rubber. Part II: physical basis of contributions to the model. Rubber Chem. Technol. 84 (1), 24–40.
Berg, M., .1995. A rubber spring model for dynamic analysis of rail vehicles, Tech. rep., Railway Technology, Department of Vehicle Engineering, Royal Institute of Technology.
Bergström, J., Boyce, M., 1998. Constitutive modelling of the large strain time-dependant behaviour of elastomers. J. Mech. Phys. Solids 46 (5), 931–954.
Besdo, D., Ihlemann, J., 2003. A phenomenological constitutive model for rubberlike materials and its numerical applications. Int. J. Plast. 19, 1019–1036.
Boyce, M., Arruda, E., 2000. Constitutive models of rubber elasticity: a review. Rubber Chem. Technol. 73, 504–523.
Chazeu, L., Brown, J., Yanyo, L., Sternstein, S., 2000. Modulus recovery kinetics and other insights into the payne effect for filled elastomers. Polym. Compos. 21 (2), 202–222.

Coveney, V., Johnson, D., 1999. Modeling of carbon black filled natural rubber vulcanizates by the standard triboelastic solid. Rubber Chem. Technol. 72, 673–683.
Coveney, V., Johnson, D., 2000. Rate-dependent modeling of a highly filled vulcanizate. Rubber Chem. Technol. 73, 565–577.
Coveney, V., Johnsson, D., Turner, D., 1995. A triboelastic model for the cyclic mechanical behaviour of filled vulcanizates. Rubber Chem. Technol. 68, 660–670.
Dafalias, Y., Popov, E., 1977. Cyclic loading for materials with a vanishing elastic region. Nucl. Eng. Des. 41, 293–302.
Dahl, P., 1960. A solid friction model. Tech. Rep. TOR-158 (3107-18)-1, The Aerospace Corporation, El Segundo, CA.
Donnet, J.-B., Custodero, E., 2013. The Science and Technology of Rubber,, Academic press, The Boulevard, Langford Lane, Kidlington, Oxford, OX5 1GB, UK, Ch. Reinforcement of Elastomers by Particulate Fillers, pp. 383–416.
Edwards, S., Vilgis, T., 1998. The tube model theory of rubber elasticity. Rep. Prog. Phys. 51, 243–297.
Fletcher, W., Gent, A., 1953. Nonlinearity in the dynamic properties of vulcanized rubber compounds. Trans. Inst. Rubber Ind. 29 (5), 266–280.
Fröhlich, J., Niedermeier, W., Luginsland, H.-D., 2005. The effect of filler–filler and filler–elastomer interaction on rubber reinforcement. Compos. Part A 36, 449460.
García Tárrago, M., Kari, L., Vinolas, J., Gil-Negrete, N., 2007. Frequency and amplitude dependence of the axial and radial stiffness of carbon-black filled rubber bushings. Polym. Test. 26, 629–638.
Govindjee, S., Reese, S., 1997. A presentation and comparison of two large deformation viscoelasticity models. J. Eng. Mater. Technol. 119, 251–255.
Gracia, L., Liarte, E., Pelegay, J., Calvo, B., 2010. Finite element simulation of the hysteretic behaviour of an industrial rubber. Application to design of rubber components. Finite Elem. Anal. Des. 46, 357–368.
Heinrich, G., Klüppel, M., 2002. Recent advances in the theory of filler networking in elastomers. Adv. Polym. Sci. 160, 1–44.
Heinrich, G., Klüppel, M., Vilgis, T., 2002. Reinforcement of elastomers. Solid State Mater. Sci. 6, 195–203.
Höfer, P., Lion, A., 2009. Modelling of frequency- and amplitude-dependent material properties of filler-reinforced rubber. J. Mech. Phys. Solids 57, 500–520.
Hu, W., Wereley, N.M., 2012. Advanced Elastomers – Technology, Properties and Applications, InTech, 2012, Ch. Anelastic Behavior in Filled Elastomers Under Harmonic Loading Using Distributed Rate-Dependent Elasto-Slide Elements, pp. 307–340.
Kraus, G., 1984. Mechanical losses in carbon-black-filled rubbers. J. Appl. Polym. Sci.: Appl. Polym. Symp. 39, 75–92.
Lion, A., 1998. Thixotropic behaviour of rubber under dynamic loading histories: Experiments and theory. J. Mech. Phys. Solids 46 (5), 895–930.
Lion, A., Kardelky, C., 2004. The payne effect in finite viscoelasticity: constitutive modelling based on fractional derivatives and intrinsic time scales. Int. J. Plast. 20, 1313–1345.
Litvinov, V., Orza, R., Klüppel, M., van Duin, M., Magusin, P., 2011. Rubber-filler interactions and network structure in relation to stress-strain behavior of vulcanized, carbon black filled epdm. Macromolecules 44, 4887–4900.
Liu, M., Fatt, M.S.H., 2011. A constitutive equation for filled rubber under cyclic loading. Int. J. Non-Linear Mech. 46, 446–456.
Luo, W., Hua, X., Wang, C., Li, Q., 2010. Frequency- and strain-amplitude-dependent dynamical mechanical properties and hysteresis loss of cb-filled vulcanized natural rubber. Int. J. Mech. Sci. 52, 168–174.
Mullins, L., 1969. Softening of rubber by deformation. Rubber Chem. Technol. 42 (1), 339–362.
Netzker, C., Dal, H., Kaliske, M., 2010. An endochronic plasticity formulation for filled rubber. Int. J. Solids Struct. 47, 2371–2379.
Ottosen, N.S., Ristinmaa, M., 2005. The Mechanics of Constitutive Modeling. Elsevier Ltd.
Payne, A., 1962. The dynamic properties of carbon black-loaded natural rubber vulcanizates. part i. J. Appl. Polym. Sci. VI (19), 57–63.
Rendek, M., Lion, A., 2010. Amplitude dependence of filler-reinforced rubber: experiments, constitutive modelling and fem–implementation. Int. J. Solids Struct. 47, 2918–2936.
Rubber, 2011. Vulcanized or thermoplastic–determination of shear modulus and adhesion to rigid plates – quadruple-shear methods (ISO 1827:2011, IDT).
Sheridan, P., James, F., Miller, T., 2001. Engineering with Rubber: How to Design Rubber Components,, Carl Hanser Verlag, Ch. 8, pp. 223–255.
Sjöberg, M., Kari, L., 2002. Non-linear behaviour of a rubber isolator system using fractional derivatives. Veh. Syst. Dyn. 37 (3), 217–236.
Sjöberg, M., Kari, L., 2003. Testing of nonlinear interaction effects of sinusoidal and noise excitation on rubber isolator stiffness. Polym. Test. 22, 343–351.
Treloar, L., 2005. The Physics of Rubber Elasticity. Oxford University Press, UK.
Wrana, C., Härtel, V., 2008. Dynamic mechanical analysis of filled elastomers. KGK – Kautschuk Gummi Kunststoffe, 647–655, December.
Yarmohamadi, H., Berbyuk, V., 2010. Computational model of conventional engine mounts for commercial vehicles: validation and application. Veh. Syst. Dyn. 49 (5), 761–787.